

Production of Single W Bosons at $\sqrt{s} = 189$ GeV and Measurement of $WW\gamma$ Gauge Couplings

The L3 Collaboration

Abstract

Single W boson production in electron-positron collisions is studied with the L3 detector at LEP. The data sample collected at a centre-of-mass energy of $\sqrt{s} = 188.7$ GeV corresponds to an integrated luminosity of 176.4 pb^{-1} . Events with a single energetic lepton or two acoplanar hadronic jets are selected. Within phase-space cuts, the total cross-section is measured to be $0.53 \pm 0.12 \pm 0.03 \text{ pb}$, consistent with the Standard Model expectation. Including our single W boson results obtained at lower \sqrt{s} , the $WW\gamma$ gauge couplings κ_γ and λ_γ are determined to be $\kappa_\gamma = 0.93 \pm 0.16 \pm 0.09$ and $\lambda_\gamma = -0.31^{+0.68}_{-0.19} \pm 0.13$.

Submitted to *Phys. Lett. B*

1 Introduction

Precise measurements of trilinear gauge boson couplings constitute a crucial test of the Standard Model of electroweak interactions [1, 2]. The studies of single W production¹⁾

$$e^+e^- \rightarrow e^+\nu_e W^- \quad (1)$$

by the LEP experiments [3–6] demonstrated that this process provides one of the best experimental grounds for precision measurements of the electromagnetic gauge couplings of the W boson. The cross-section of process (1) depends only on the κ_γ and λ_γ gauge coupling parameters [7] which are related to the magnetic dipole moment, $\mu_W = (e/(2m_W))(1 + \kappa_\gamma + \lambda_\gamma)$, and the electric quadrupole moment, $Q_W = (-e/m_W^2)(\kappa_\gamma - \lambda_\gamma)$, of the W boson. Any deviation from the Standard Model predictions $\kappa_\gamma = 1$ and $\lambda_\gamma = 0$ would indicate that the W boson has an internal structure.

A specific feature of this reaction is a final state positron produced at very low polar angle and therefore not detected. Thus the signature of this process is a single energetic lepton, if the W^- boson decays into lepton and anti-neutrino, or two hadronic jets and large transverse momentum imbalance in case of hadronic W^- decay.

In this article we report on the measurement of the cross-section of single W boson production at a centre-of-mass energy of $\sqrt{s} = 188.7$ GeV, denoted hereafter as $\sqrt{s} = 189$ GeV. Combining these results with those on single W boson production obtained at lower \sqrt{s} [4], we derive significantly more precise values for the gauge couplings κ_γ and λ_γ .

2 Data and Monte Carlo Samples

The data were collected by the L3 detector [8] at LEP in 1998 with an integrated luminosity of 176.4 pb^{-1} .

For signal studies samples of $e^+e^- \rightarrow e^+\nu_e f \bar{f}'$ events are generated using both the GRC4F [9] and the EXCALIBUR [10] Monte Carlo generators. For the background studies the following Monte Carlo programs are used: KORALW [11] ($e^+e^- \rightarrow W^+W^- \rightarrow ffff$), KORALZ [12] ($e^+e^- \rightarrow \mu^+\mu^-(\gamma)$, $\tau^+\tau^-(\gamma)$), BHAGENE3 [13] and BHWIDE [14] for large angle Bhabha scattering ($e^+e^- \rightarrow e^+e^-(\gamma)$), TEEGG [15] for small angle Bhabha scattering ($e^+e^- \rightarrow e^+e^-\gamma$), PYTHIA [16] ($e^+e^- \rightarrow q\bar{q}(\gamma)$), DIAG36 [17] and PHOJET [18] for leptonic and hadronic two-photon processes, respectively, and EXCALIBUR and GRC4F for other 4-fermion final states.

The Monte Carlo events are simulated in the L3 detector using the GEANT 3.15 program [19], which takes into account the effects of energy loss, multiple scattering and showering in the detector. The GHEISHA program [20] is used to simulate hadronic interactions in the detector.

3 Signal Definition

The signal definition used here is unchanged with respect to our previous publications [3, 4]. The signal is defined as $e^+e^- \rightarrow e^+\nu_e f \bar{f}'$ events that satisfy the following phase-space cuts:

¹⁾The charge conjugate reactions are understood to be included throughout the paper.

$$\begin{aligned}
|\cos\theta_{e^+}| &> 0.997 \\
\min(E_f, E_{\bar{f}'}) &> 15 \text{ GeV} \\
|\cos\theta_{e^-}| &< 0.75 \quad \text{for } e^+\nu_e e^-\bar{\nu}_e \text{ events only,}
\end{aligned}
\tag{2}$$

where θ_{e^+} is the polar angle of the outgoing positron, and E_f and $E_{\bar{f}'}$ are the fermion energies. The final states $e^+e^- \rightarrow e^+\nu_e f\bar{f}'$ that do not satisfy these conditions are considered as background; they consist mostly of the reaction $e^+e^- \rightarrow W^+W^-$. In the case of the $e^+\nu_e e^-\bar{\nu}_e$ final state the additional angular cut reduces contributions from processes where the $\nu_e\bar{\nu}_e$ pair originates from the decay of a Z boson.

Inside the phase-space region (2), single W production dominates since it peaks strongly at $|\cos\theta_{e^+}| \sim 1$. On average it accounts for 90% of all events in this region, the remaining 10% being mostly non-resonant final states. The purity depends slightly on the flavour of the $f\bar{f}'$ pair from W^- decays. For the $e^+\nu_e e^-\bar{\nu}_e$ final state, the purity is 75%.

For comparison with theory, the cross-sections for this signal definition are calculated with a statistical precision from 0.2% to 1.0% using the Monte Carlo generators GRC4F and EXCALIBUR. The main difference between the two generators is the approximation of massless fermions used in EXCALIBUR. The reduction of theoretical uncertainties on predictions for single W production is subject to ongoing theoretical efforts [21]. With respect to this discussion, we estimate the theoretical uncertainty on the calculated cross-section for single W production to be of the order of 7%. This includes the effect of using a smaller electromagnetic coupling accounting for the low momentum transfer of the photon in single W production and taking into account QED radiative corrections expected for such a t -channel process. Rescaling with respect to a smaller electromagnetic coupling constant would lower the cross section by 7% to 10%, whereas replacing the energy scale used in the structure function approach to calculate QED corrections with the correct physical scale is expected to increase the cross-section by about 5%.

4 Analysis

All decay modes of the W boson are considered, leading to the following experimental signatures: events with two hadronic jets and large transverse momentum imbalance and events with single energetic electrons, muons and taus. In the following, efficiencies are quoted with respect to the phase-space cuts (2), with errors due to Monte Carlo statistics.

4.1 Hadronic Final States

The selection of candidates for the hadronic decay $W^- \rightarrow q\bar{q}'$ of single W boson production is based on the following requirements: two acoplanar hadronic jets, no leptons, and large transverse momentum imbalance.

High multiplicity hadronic events with at least five charged tracks are selected with an energy deposition in the electromagnetic calorimeter greater than 10 GeV and large total visible energy, $E_{\text{vis}} > 60$ GeV. All calorimetric clusters in the event are forced to two hadronic jets using the DURHAM jet finding algorithm [22]. The invariant mass of the jet-jet system must be in the range $40 \text{ GeV} < M_{\text{vis}} < 110 \text{ GeV}$. The energy E_{FB} in the forward-backward luminosity calorimeters, covering the angular range $0.025 \text{ rad} < \theta < 0.151 \text{ rad}$, where θ is measured with respect to the incoming electron or positron, is required to be smaller than 65 GeV. These cuts

reduce contributions from the purely leptonic final states $e^+e^- \rightarrow e^+e^-(\gamma)$, $\mu^+\mu^-(\gamma)$, $\tau^+\tau^-(\gamma)$ and hadronic two-photon interactions while keeping a significant fraction of hadronic events from the processes $e^+e^- \rightarrow q\bar{q}(\gamma)$, $e^+e^- \rightarrow W^+W^-$ and $e^+e^- \rightarrow ZZ$.

To reject events from the two-fermion production process $e^+e^- \rightarrow q\bar{q}(\gamma)$, the missing transverse momentum must exceed 15 GeV. The missing momentum vector must be at least 0.30 rad away from the beam axis and the energy in the ± 0.22 rad azimuthal sector around its direction must be below 10 GeV. In addition, the opening angle between the two jets in the plane perpendicular to the beam axis must be smaller than 3.0 rad.

Events containing identified electrons, muons or photons with energy greater than 20 GeV are rejected in order to suppress the remaining background from $e^+e^- \rightarrow W^+W^-$ events where one of the W bosons decays into leptons. In order to remove part of the remaining $\tau^+\nu_\tau q\bar{q}'$ final states with the τ lepton decaying hadronically, the event is forced to a three-jet topology using the DURHAM algorithm. The solid angle, Ω , defined by the directions of these jets is required to be smaller than 5.5 sr.

At 189 GeV centre-of-mass energy, the production of two on-mass-shell Z bosons is a source of an additional background. A decay of one Z into neutrinos accompanied by a hadronic decay of the other Z leads to an event signature close to that of the signal process (1). To suppress this background, we make use of the fact that the Z bosons produced in pairs are close to the kinematic threshold and therefore have low momenta. Thus we ask the velocity of the detected hadronic system, β , calculated as the ratio of the missing momentum to the visible energy to be greater than 0.35.

A total of 216 events are observed in the data, with 35.9 events expected from the signal according to the EXCALIBUR Monte Carlo prediction and 179 from the background sources distributed as follows: W^+W^- production and non resonant $e^+\nu_e q\bar{q}'$ final states (166.2 events), ZZ production (7 events), two-fermion final state processes (4.2 events) and two-photon interactions (1.5 events). The contributions to the background from other processes are found to be negligible. The number of observed events is in good agreement with the expectation. The signal selection efficiency is determined to be $(50.5 \pm 0.7)\%$ using the EXCALIBUR Monte Carlo and $(51.8 \pm 1.3)\%$ using GRC4F Monte Carlo.

In order to differentiate further between the signal and the W^+W^- background, a discriminant variable NN_{out} is constructed using a neural network. Nine variables are combined in a feed-forward neural network [23], with one hidden layer and one output node. The input to the neural net includes the sphericity of the event, the invariant mass of the two jets, the masses of the two jets, the velocity β of the hadronic system, the solid angle Ω , the resolution parameters y_{23} and y_{34} of the JADE jet finding algorithm [24] for which the number of jets in the event changes from two to three and three to four, respectively, and the ratio of the mass to the energy of the least energetic jet after forcing the event to three jets. As an example, the distribution of the solid angle Ω for the selected events is shown in Figure 1(a). The use of the neural network increases the signal fraction in the selected sample to approximately 60% for large neural network output values, as shown in Figure 1(b).

The cross-section of the process (1) for hadronic decays of the W boson is determined by a binned log-likelihood fit to the neural network output distribution of Figure 1(b), assuming Poisson statistics. The background contributions are fixed to the corresponding Standard Model Monte Carlo predictions. The fitted cross-section of the hadron channel is found to be:

$$\sigma(e^+e^- \rightarrow e\nu_e qq) = 0.41 \pm 0.11 \text{ pb.}$$

A similar result is obtained if the GRC4F Monte Carlo is used for the simulation of the signal.

This result has to be compared with the expected signal cross-section of 0.40 pb predicted by EXCALIBUR and 0.38 pb predicted by GRC4F.

As a check of the analysis procedure, a fit of the total W^+W^- cross-section, keeping the single W contribution fixed to the EXCALIBUR Monte Carlo prediction, gives the value 16.9 ± 1.5 pb in good agreement with the Standard Model expectation of 16.7 pb predicted by KORALW. The result of the fit with both W^+W^- and single W production cross-sections as free parameters is in good agreement with the results above.

4.2 Leptonic Final States

The distinct feature of the process $e^+e^- \rightarrow e^+\nu_e W^-$, $W^- \rightarrow \ell^- \bar{\nu}_\ell$ is a high energy lepton from W decay with no other significant activity in the detector.

Events with one charged lepton (electron, muon or tau) with an energy of at least 15 GeV are selected. The lepton identification is based on the energy distribution in the electromagnetic and hadron calorimeters associated with the trajectory of charged particles. The total energy, E_{vis} , is calculated as the sum of the lepton energy, E_ℓ , measured as discussed below, and the energies of all neutral calorimetric clusters in the event. No other charged particle activity is allowed. The ratio E_ℓ/E_{vis} is required to exceed 0.92 in order to suppress background from two-fermion production $e^+e^- \rightarrow \ell^+\ell^-(\gamma)$. In addition, the energy in the ± 0.22 rad azimuthal angle sector along the missing energy direction must be below 1 GeV (0.2 GeV for muons). The energy in the forward-backward luminosity calorimeters, E_{FB} , must be less than 70 GeV. The accepted background is dominated by two-fermion production processes, especially radiative Bhabha scattering in the case of the single electron final state, $e^+\nu_e e^- \bar{\nu}_e$. Moreover, significant contributions are due to 4-fermion final states that include two neutrinos and fall outside the signal definition (2).

4.2.1 Single Electron Final States

Electrons are identified as clusters in the electromagnetic calorimeter consistent with an electromagnetic shower shape matched in azimuthal angle with a track reconstructed in the central tracker. For the single electron final states, the electron energy, E_e , measured in the electromagnetic calorimeter, must exceed 20 GeV and the polar angle θ_e must satisfy the condition $|\cos \theta_e| < 0.7$. This requirement reduces the contribution from Bhabha and Compton scattering and from the process $e^+e^- \rightarrow e^+e^- \nu \bar{\nu}$ where the e^+e^- pair originates from a low-mass virtual photon. The $e^+e^- \rightarrow e^+e^-(\gamma)$ events constitute the dominant contribution to the selected sample. The requirements $E_e/E_{\text{vis}} > 0.92$ and $E_{\text{FB}} < 70$ GeV reduce significantly this contribution. The acoplanarity angle between the direction of the electron and the most energetic neutral cluster (if any) must be greater than 0.14 rad.

A total of 8 events are observed with 11.9 expected from the Standard Model including 7.9 events expected from the signal as predicted by the EXCALIBUR Monte Carlo. The energy spectrum of the selected events is presented in Figure 2(a).

The trigger efficiency is found to be 92% from a control data sample. The signal selection efficiency is estimated to be $(80 \pm 2)\%$ using the EXCALIBUR Monte Carlo program and $(78 \pm 3)\%$ using GRC4F. The major sources of the efficiency loss are due to the requirements $|\cos \theta_e| < 0.7$ and $E_e > 20$ GeV. A binned log-likelihood fit to the electron energy spectrum results in:

$$\sigma(e^+e^- \rightarrow e\nu_e e\nu_e) = 0.021_{-0.020}^{+0.026} \text{ pb} ,$$

to be compared with the signal cross-section of 0.056 pb predicted by EXCALIBUR and 0.054 pb predicted by GRC4F.

4.2.2 Single Muon Final States

Single muon final states are selected as events containing one isolated muon, identified as a reconstructed track in the muon chambers and the central tracker. The muon energy, E_μ , measured in the muon chambers and in the central tracker, is required to exceed 15 GeV. The fiducial volume for this analysis is defined to be $|\cos\theta_\mu| < 0.85$. This latter requirement avoids significant decrease of the trigger efficiency for single muons in the angular region $|\cos\theta_\mu| > 0.85$. Within the acceptance, the trigger efficiency exceeds 96%. The total calorimetric energy not associated to the muon must not exceed 3 GeV. The rejection of background from cosmic muons is based on the radial distance of closest approach of the muon to the beam line and a match in azimuthal angle of the muon chamber track with a track reconstructed in the central tracker.

A total of 10 events are observed with 9.8 expected from Standard Model processes including 7.5 events from the signal. The energy spectrum of the selected single muon candidates is presented in Figure 2(b). A signal efficiency of $(61 \pm 2)\%$ is estimated using the EXCALIBUR Monte Carlo program and $(56 \pm 2)\%$ using GRC4F. The main source of the efficiency loss is due to the geometrical acceptance of the muon chambers. A binned log-likelihood fit to the muon energy spectrum results in:

$$\sigma(e^+e^- \rightarrow e\nu_e\mu\nu_\mu) = 0.070_{-0.027}^{+0.034} \text{ pb} .$$

The expected signal cross-section is 0.060 pb according to EXCALIBUR and 0.059 pb according to GRC4F.

4.2.3 Single Tau Final States

Single tau final states are selected as events containing one low-multiplicity hadronic jet. The calorimetric energy associated with the τ jet, E_τ , must exceed 15 GeV. The number of tracks reconstructed in the central tracking system must be either 1 or 3.

A total of 4 events are observed with 3.6 expected from the Standard Model processes including 2.1 events from the signal. The energy spectrum of selected single tau candidates is presented in Figure 2(c). The signal efficiency is estimated to be $(26 \pm 2)\%$ using EXCALIBUR and $(29 \pm 2)\%$ using GRC4F. The trigger efficiency was studied and found to be in excess of 98%. A binned log-likelihood fit to the tau energy spectrum yields:

$$\sigma(e^+e^- \rightarrow e\nu_e\tau\nu_\tau) = 0.066_{-0.050}^{+0.073} \text{ pb} .$$

The predictions for the signal cross-section are 0.060 pb and 0.059 pb according to EXCALIBUR and GRC4F, respectively.

5 Systematic Uncertainties

In case of the hadronic decay of the single W, the differences of the EXCALIBUR and GRC4F signal modelling are taken into account in the systematic uncertainty of the cross-section measurement. This systematic uncertainty is found to be approximately 3%. In addition, the

parameters describing the neural network structure are varied and the analysis is repeated to allow an estimation of the uncertainty due to the choice of the network, yielding a contribution of 3%. Compared to this, detector effects, studied by smearing and shifting the kinematic variables that are fed into the network within the experimental resolution, have a negligible impact on the result.

In the lepton channel, the dominant systematic uncertainty of approximately 4% arises from the signal modelling comparing the signal efficiencies estimated using EXCALIBUR and GRC4F. The uncertainty due to the identification of leptons is studied using control data samples of two-fermion production and is found to be less than 1.5%.

The uncertainty due to the Monte Carlo signal statistics ranges from 1% to 3% on the cross-section depending on the decay channel. The systematic uncertainty on the expected number of background events is essentially due to the limited Monte Carlo statistics, with smaller contributions from the uncertainties on the cross-sections and the selection efficiencies for the background processes. The overall uncertainty on the total number of background events ranges from 3% to 4% in the individual channels. These uncertainties are uncorrelated among individual channels and different centre-of-mass energies and have negligible impact on the final results. Taking into account all the contributions, the systematic uncertainty of the cross-section measurement amounts to 5% for the hadronic decay channel and 6% overall.

6 Results

6.1 Total Cross-Section

The total cross-section of single W production is determined from a binned likelihood fit to the distributions of the neural network output presented in Figure 1(b) and the lepton energy spectra shown in Figures 2(a) – (c). The sum of the different lepton energy distributions is presented in Figure 2(d). The background shapes and normalisations are fixed to the Monte Carlo prediction. The fitted signal cross-section, $\sigma(e^+e^- \rightarrow e\nu_e W)$, corresponds to that of the process $e^+e^- \rightarrow e\nu_e ff$, where ff denotes a sum of all $\ell\nu_\ell$ and qq final states satisfying the phase-space conditions (2). The total single W boson cross-section at $\sqrt{s} = 189$ GeV is then determined to be:

$$\sigma(e^+e^- \rightarrow e\nu_e W) = 0.53 \pm 0.12 \pm 0.03 \text{ pb},$$

where the first error is statistical and the second systematic. The measured cross-section value is consistent with the Standard Model prediction of 0.57 pb calculated with EXCALIBUR and 0.56 pb calculated with GRC4F. The dependence of the cross-section on the centre-of-mass energy agrees well with the Monte Carlo predictions as shown in Figure 3, including our previous measurements at centre-of-mass energies between 130 GeV and 183 GeV [4].

6.2 WW γ Gauge Couplings

The electromagnetic gauge couplings κ_γ and λ_γ describing the WW γ vertex are determined from a binned maximum-likelihood fit similar to the one used for the cross section determination. In the fit each Monte Carlo event is assigned a weight that depends on the generated 4-fermion event kinematics and the values of the gauge couplings κ_γ and λ_γ . The dependence of the background from W^+W^- production on the gauge couplings is also taken into account. The weight is calculated using the matrix element as implemented in EXCALIBUR, imposing constraints on the triple gauge boson couplings κ_Z and λ_Z arising from the $SU(2) \times U(1)$ gauge

invariance: $\kappa_Z = g_1^Z - \tan^2 \theta_w (\kappa_\gamma - 1)$ and $\lambda_Z = \lambda_\gamma$. These constraints affect only the background contributions, as the signal process depends on λ_γ and κ_γ only. The general analysis of the remaining C- and P-conserving couplings, g_1^Z , λ_γ and κ_γ , can only be done with full consideration of the W^+W^- production. In the present analysis we fix the weak charge of the W bosons to its Standard Model value, $g_1^Z = 1$, and focus on the electromagnetic properties of W bosons.

The dependence of the coupling determination on the total cross-section for single W boson production is tested repeating the likelihood fit with a $\pm 7\%$ variation of the signal cross-section. The corresponding systematic uncertainty is ± 0.04 for κ_γ and ± 0.02 for λ_γ . Comparing the signal description of the two Monte Carlo Generators, EXCALIBUR and GRC4F, shows an additional systematic uncertainty of ± 0.05 and ± 0.06 on κ_γ and λ_γ , respectively. The agreement between the two generators for various anomalous couplings is checked. No coupling-dependence of the ratio of the two cross-section predictions was found.

In addition, the cross-section of the background contributions coming from W^+W^- and ZZ production are varied to allow an estimation of the systematic uncertainty. The influence of these uncertainties on the coupling determination is found to be less than ± 0.02 .

The estimated systematic uncertainty is assumed to be Gaussian and fully correlated between individual channels. The systematic uncertainty in the cross-section determination is taken into account by convolution of the likelihood function with a Gaussian in the fit.

For the fit to the couplings, we combine the single W data at $\sqrt{s} = 189$ GeV presented here with our single W data already published [4]. Single W boson production is particularly sensitive to the gauge coupling κ_γ . Thus, this coupling is determined in a fit fixing $\lambda_\gamma = 0$ to be:

$$\kappa_\gamma = +0.96_{-0.17}^{+0.15} \pm 0.09,$$

where the first error is statistical and the second systematic. Fixing $\kappa_\gamma = 1$ and performing a fit for λ_γ yields:

$$\lambda_\gamma = -0.26_{-0.19}^{+0.53} \pm 0.13.$$

Varying both couplings λ_γ and κ_γ freely in the fit yields:

$$\begin{aligned} \kappa_\gamma &= +0.93 \pm 0.16 \pm 0.09 \\ \lambda_\gamma &= -0.31_{-0.19}^{+0.68} \pm 0.13, \end{aligned}$$

with a correlation coefficient of $+37\%$. The 68% and 95% confidence level contours on κ_γ and λ_γ are shown in Figure 4. The results are consistent with the absence of anomalous contributions to $WW\gamma$ couplings. The limits on κ_γ and λ_γ at 95% confidence level are:

$$\begin{aligned} 0.56 &< \kappa_\gamma < 1.29 & \text{for } \lambda_\gamma = 0 \\ -0.67 &< \lambda_\gamma < 0.59 & \text{for } \kappa_\gamma = 1. \end{aligned}$$

These results represent a major improvement in the accuracy on the triple gauge boson couplings κ_γ and λ_γ compared to our previous publications on single W boson production [3, 4]. They are complementary to measurements based on W^+W^- production at LEP [6, 25] or determined at the Tevatron $p\bar{p}$ collider [26].

Acknowledgements

We wish to express our gratitude to the CERN accelerator divisions for the excellent performance of the LEP machine. We acknowledge the efforts of the engineers, technicians and support staff who have participated in the construction and maintenance of this experiment.

Author List

The L3 Collaboration:

M.Acciarri²⁶ P.Achard¹⁹ O.Adriani¹⁶ M.Aguilar-Benitez²⁵ J.Alcaraz²⁵ G.Alemanni²² J.Allaby¹⁷ A.Aloisio²⁸
M.G.Alvigi²⁸ G.Ambrosi¹⁹ H.Anderhub⁴⁸ V.P.Andreev^{6,36} T.Angelescu² F.Anselmo⁹ A.Arefiev²⁷ T.Azmoon³
T.Aziz¹⁰ P.Bagnaia³⁵ A.Bajo²⁵ L.Baksay⁴³ A.Balandras⁴ S.V.Baldew² S.Banerjee¹⁰ Sw.Banerjee¹⁰
A.Barczyk^{48,46} R.Barillère¹⁷ L.Barone³⁵ P.Bartalini²² M.Basile⁹ R.Battiston³² A.Bay²² F.Becattini¹⁶ U.Becker¹⁴
F.Behner⁴⁸ L.Bellucci¹⁶ R.Berbeco³ J.Berdugo²⁵ P.Berges¹⁴ B.Bertucci³² B.L.Betev⁴⁸ S.Bhattacharya¹⁰
M.Biasini³² A.Biland⁴⁸ J.J.Blaising⁴ S.C.Blyth³³ G.J.Bobbink² A.Böhm¹ L.Boldizsar¹³ B.Borgia³⁵ D.Bourilkov⁴⁸
M.Bourquin¹⁹ S.Braccini¹⁹ J.G.Branson³⁹ V.Brigljevic⁴⁸ F.Brochu⁴ A.Buffini¹⁶ A.Buijs⁴⁴ J.D.Burger¹⁴
W.J.Burger³² X.D.Cai¹⁴ M.Campanelli⁴⁸ M.Capell¹⁴ G.Cara Romeo⁹ G.Carlino²⁸ A.M.Cartacci¹⁶ J.Casaus²⁵
G.Castellini¹⁶ F.Cavallari³⁵ N.Cavallo³⁷ C.Cecchi³² M.Cerrada²⁵ F.Cesaroni²³ M.Chamizo¹⁹ Y.H.Chang⁵⁰
U.K.Chaturvedi¹⁸ M.Chemarin²⁴ A.Chen⁵⁰ G.Chen⁷ G.M.Chen⁷ H.F.Chen²⁰ H.S.Chen⁷ G.Chiefari²⁸
L.Cifarelli³⁸ F.Cindolo⁹ C.Civinini¹⁶ I.Clare¹⁴ R.Clare¹⁴ G.Coignet⁴ N.Colino²⁵ S.Costantini⁵ F.Cotorobai¹²
B.de la Cruz²⁵ A.Csilling¹³ S.Cucciarelli³² T.S.Dai¹⁴ J.A.van Dalen³⁰ R.D'Alessandro¹⁶ R.de Asmundis²⁸
P.Déglon¹⁹ A.Degré⁴ K.Deiters⁴⁶ D.della Volpe²⁸ E.Delmeire¹⁹ P.Denes³⁴ F.DeNotaristefani³⁵ A.De Salvo⁴⁸
M.Diemoz³⁵ M.Dierckxsens² D.van Dierendonck² F.Di Lodovico⁴⁸ C.Dionisi³⁵ M.Dittmar⁴⁸ A.Dominguez³⁹
A.Doria²⁸ M.T.Dova^{18,†} D.Duchesneau⁴ D.Dufournaud⁴ P.Duinker² I.Duran⁴⁰ H.El Mamouni²⁴ A.Engler³³
F.J.Eppling¹⁴ F.C.Erne² P.Extermann¹⁹ M.Fabre⁴⁶ R.Faccini³⁵ M.A.Falagan²⁵ S.Falciano^{35,17} A.Favara¹⁷ J.Fay²⁴
O.Fedin³⁶ M.Felcini⁴⁸ T.Ferguson³³ F.Ferroni³⁵ H.Fesefeldt¹ E.Fiandrini³² J.H.Field¹⁹ F.Filthaut¹⁷ P.H.Fisher¹⁴
I.Fisk³⁹ G.Forconi¹⁴ K.Freudenreich⁴⁸ C.Furetta²⁶ Yu.Galaktionov^{27,14} S.N.Ganguli¹⁰ P.Garcia-Abia⁵
M.Gataullin³¹ S.S.Gau¹¹ S.Gentile^{35,17} N.Gheordanescu¹² S.Giagu³⁵ Z.F.Gong²⁰ G.Grenier²⁴ O.Grimm⁴⁸
M.W.Gruenewald⁸ M.Guida³⁸ R.van Gulik² V.K.Gupta³⁴ A.Gurtu¹⁰ L.J.Gutay⁴⁵ D.Haas⁵ A.Hasan²⁹
D.Hatzifotiadou⁹ T.Hebbeker⁸ A.Hervé¹⁷ P.Hidas¹³ J.Hirschfelder³³ H.Hofer⁴⁸ G.Holzner⁴⁸ H.Hoorani³³
S.R.Hou⁵⁰ Y.Hu³⁰ I.Iashvili⁴⁷ B.N.Jin⁷ L.W.Jones³ P.de Jong² I.Josa-Mutuberría²⁵ R.A.Khan¹⁸ M.Kaur^{18,◇}
M.N.Kienzle-Focacci¹⁹ D.Kim³⁵ J.K.Kim⁴² J.Kirkby¹⁷ D.Kiss¹³ W.Kittel³⁰ A.Klimentov^{14,27} A.C.König³⁰
A.Kopp⁴⁷ V.Koutsenko^{14,27} M.Kräber⁴⁸ R.W.Kraemer³³ W.Krenz¹ A.Krüger⁴⁷ A.Kunin^{14,27}
P.Ladron de Guevara²⁵ I.Laktineh²⁴ G.Landi¹⁶ K.Lassila-Perini⁴⁸ M.Lebeau¹⁷ A.Lebedev¹⁴ P.Lebrun²⁴
P.Lecomte⁴⁸ P.Lecod¹⁷ P.Le Coultre⁴⁸ H.J.Lee⁸ J.M.Le Goff¹⁷ R.Leiste⁴⁷ E.Leonardi³⁵ P.Levtchenko³⁶ C.Li²⁰
S.Likhoded⁴⁷ C.H.Lin⁵⁰ W.T.Lin⁵⁰ F.L.Linde² L.Lista²⁸ Z.A.Liu⁷ W.Lohmann⁴⁷ E.Longo³⁵ Y.S.Lu⁷
K.Lübelsmeyer¹ C.Luci^{17,35} D.Luckey¹⁴ L.Lugnier²⁴ L.Luminari³⁵ W.Lustermann⁴⁸ W.G.Ma²⁰ M.Maity¹⁰
L.Malgeri¹⁷ A.Malinin¹⁷ C.Maña²⁵ D.Mangeol³⁰ J.Mans³⁴ P.Marchesini⁴⁸ G.Marian¹⁵ J.P.Martin²⁴ F.Marzano³⁵
K.Mazumdar¹⁰ R.R.McNeil⁶ S.Mele¹⁷ L.Merola²⁸ M.Meschini¹⁶ W.J.Metzger³⁰ M.von der Mey¹ A.Mihul¹²
H.Milcent¹⁷ G.Mirabelli³⁵ J.Mnich¹⁷ G.B.Mohanty¹⁰ P.Molnar⁸ T.Moulik¹⁰ G.S.Muanza²⁴ A.J.M.Muijs²
B.Musicar³⁹ M.Musy³⁵ M.Napolitano²⁸ F.Nessi-Tedaldi⁴⁸ H.Newman³¹ T.Niessen¹ A.Nisati³⁵ H.Nowak⁴⁷
G.Organtini³⁵ A.Oulianov²⁷ C.Palomares²⁵ D.Pandoulas¹ S.Paoletti^{35,17} P.Paolucci²⁸ R.Paramatti³⁵ H.K.Park³³
I.H.Park⁴² G.Passaleva¹⁷ S.Patricelli²⁸ T.Paul¹¹ M.Pauluzzi³² C.Paus¹⁷ F.Pauss⁴⁸ M.Pedace³⁵ S.Pensotti²⁶
D.Perret-Gallix⁴ B.Petersen³⁰ D.Piccolo²⁸ F.Pierella⁹ M.Pieri¹⁶ P.A.Piroué³⁴ E.Pistoletti²⁶ V.Plyaskin²⁷ M.Pohl¹⁹
V.Pojidaev^{27,16} H.Postema¹⁴ J.Pothier¹⁷ D.O.Prokofiev⁴⁵ D.Prokofiev³⁶ J.Quartieri³⁸ G.Rahal-Callot^{48,17}
M.A.Rahaman¹⁰ P.Raics¹⁵ N.Raja¹⁰ R.Ramelli⁴⁸ P.G.Rancoita²⁶ A.Raspereza⁴⁷ G.Raven³⁹ P.Razis²⁹ D.Ren⁴⁸
M.Rescigno³⁵ S.Reucroft¹¹ S.Riemann⁴⁷ K.Riles³ A.Robohm⁴⁸ J.Rodin⁴³ B.P.Roe³ L.Romero²⁵ A.Rosca⁸
S.Rosier-Lees⁴ J.A.Rubio¹⁷ G.Ruggiero¹⁶ D.Ruschmeier⁸ H.Rykaczewski⁴⁸ S.Saremi⁶ S.Sarkar³⁵ J.Salicio¹⁷
E.Sanchez¹⁷ M.P.Sanders³⁰ M.E.Sarakinos²¹ C.Schäfer¹⁷ V.Schegelsky³⁶ S.Schmidt-Kaerst¹ D.Schmitz¹
H.Schopper⁴⁹ D.J.Schotanus³⁰ G.Schwering¹ C.Sciacca²⁸ D.Sciarrino¹⁹ A.Seganti⁹ L.Servoli³² S.Shevchenko³¹
N.Shivarov⁴¹ V.Shoutko²⁷ E.Shumilov²⁷ A.Shvorob³¹ T.Siedenburger¹ D.Son⁴² B.Smith³³ P.Spillantini¹⁶
M.Steuer¹⁴ D.P.Stickland³⁴ A.Stone⁶ B.Stoyanov⁴¹ A.Straessner¹ K.Sudhakar¹⁰ G.Sultanov¹⁸ L.Z.Sun²⁰
H.Suter⁴⁸ J.D.Swain¹⁸ Z.Szillasi^{43,¶} T.Sztaricskai^{43,¶} X.W.Tang⁷ L.Tauscher⁵ L.Taylor¹¹ B.Tellili²⁴
C.Timmermans³⁰ Samuel C.C.Ting¹⁴ S.M.Ting¹⁴ S.C.Tonwar¹⁰ J.Tóth¹³ C.Tully¹⁷ K.L.Tung⁷ Y.Uchida¹⁴
J.Ulbricht⁴⁸ E.Valente³⁵ G.Vesztegombi¹³ I.Vetlitsky²⁷ D.Vicinanza³⁸ G.Viertel⁴⁸ S.Villa¹¹ P.Violini¹⁷
M.Vivargent⁴ S.Vlachos⁵ I.Vodopianov³⁶ H.Vogel³³ H.Vogt⁴⁷ I.Vorobiev²⁷ A.A.Vorobyov³⁶ A.Vorvolakos²⁹
M.Wadhwa⁵ W.Wallraff¹ M.Wang¹⁴ X.L.Wang²⁰ Z.M.Wang²⁰ A.Weber¹ M.Weber¹ P.Wienemann¹ H.Wilkens³⁰
S.X.Wu¹⁴ S.Wynhoff¹⁷ L.Xia³¹ Z.Z.Xu²⁰ J.Yamamoto³ B.Z.Yang²⁰ C.G.Yang⁷ H.J.Yang⁷ M.Yang⁷ J.B.Ye²⁰
S.C.Yeh⁵¹ An.Zalite³⁶ Yu.Zalite³⁶ Z.P.Zhang²⁰ G.Y.Zhu⁷ R.Y.Zhu³¹ A.Zichichi^{9,17,18} G.Zilizi^{43,¶} M.Zöller¹

- 1 I. Physikalisches Institut, RWTH, D-52056 Aachen, FRG[§]
 - III. Physikalisches Institut, RWTH, D-52056 Aachen, FRG[§]
 - 2 National Institute for High Energy Physics, NIKHEF, and University of Amsterdam, NL-1009 DB Amsterdam, The Netherlands
 - 3 University of Michigan, Ann Arbor, MI 48109, USA
 - 4 Laboratoire d'Annecy-le-Vieux de Physique des Particules, LAPP, IN2P3-CNRS, BP 110, F-74941 Annecy-le-Vieux CEDEX, France
 - 5 Institute of Physics, University of Basel, CH-4056 Basel, Switzerland
 - 6 Louisiana State University, Baton Rouge, LA 70803, USA
 - 7 Institute of High Energy Physics, IHEP, 100039 Beijing, China[△]
 - 8 Humboldt University, D-10099 Berlin, FRG[§]
 - 9 University of Bologna and INFN-Sezione di Bologna, I-40126 Bologna, Italy
 - 10 Tata Institute of Fundamental Research, Bombay 400 005, India
 - 11 Northeastern University, Boston, MA 02115, USA
 - 12 Institute of Atomic Physics and University of Bucharest, R-76900 Bucharest, Romania
 - 13 Central Research Institute for Physics of the Hungarian Academy of Sciences, H-1525 Budapest 114, Hungary[‡]
 - 14 Massachusetts Institute of Technology, Cambridge, MA 02139, USA
 - 15 KLTE-ATOMKI, H-4010 Debrecen, Hungary[¶]
 - 16 INFN Sezione di Firenze and University of Florence, I-50125 Florence, Italy
 - 17 European Laboratory for Particle Physics, CERN, CH-1211 Geneva 23, Switzerland
 - 18 World Laboratory, FBLJA Project, CH-1211 Geneva 23, Switzerland
 - 19 University of Geneva, CH-1211 Geneva 4, Switzerland
 - 20 Chinese University of Science and Technology, USTC, Hefei, Anhui 230 029, China[△]
 - 21 SEFT, Research Institute for High Energy Physics, P.O. Box 9, SF-00014 Helsinki, Finland
 - 22 University of Lausanne, CH-1015 Lausanne, Switzerland
 - 23 INFN-Sezione di Lecce and Università Degli Studi di Lecce, I-73100 Lecce, Italy
 - 24 Institut de Physique Nucléaire de Lyon, IN2P3-CNRS, Université Claude Bernard, F-69622 Villeurbanne, France
 - 25 Centro de Investigaciones Energéticas, Medioambientales y Tecnológicas, CIEMAT, E-28040 Madrid, Spain^b
 - 26 INFN-Sezione di Milano, I-20133 Milan, Italy
 - 27 Institute of Theoretical and Experimental Physics, ITEP, Moscow, Russia
 - 28 INFN-Sezione di Napoli and University of Naples, I-80125 Naples, Italy
 - 29 Department of Natural Sciences, University of Cyprus, Nicosia, Cyprus
 - 30 University of Nijmegen and NIKHEF, NL-6525 ED Nijmegen, The Netherlands
 - 31 California Institute of Technology, Pasadena, CA 91125, USA
 - 32 INFN-Sezione di Perugia and Università Degli Studi di Perugia, I-06100 Perugia, Italy
 - 33 Carnegie Mellon University, Pittsburgh, PA 15213, USA
 - 34 Princeton University, Princeton, NJ 08544, USA
 - 35 INFN-Sezione di Roma and University of Rome, "La Sapienza", I-00185 Rome, Italy
 - 36 Nuclear Physics Institute, St. Petersburg, Russia
 - 37 INFN-Sezione di Napoli and University of Potenza, I-85100 Potenza, Italy
 - 38 University and INFN, Salerno, I-84100 Salerno, Italy
 - 39 University of California, San Diego, CA 92093, USA
 - 40 Dept. de Física de Partículas Elementales, Univ. de Santiago, E-15706 Santiago de Compostela, Spain
 - 41 Bulgarian Academy of Sciences, Central Lab. of Mechatronics and Instrumentation, BU-1113 Sofia, Bulgaria
 - 42 Laboratory of High Energy Physics, Kyungpook National University, 702-701 Taegu, Republic of Korea
 - 43 University of Alabama, Tuscaloosa, AL 35486, USA
 - 44 Utrecht University and NIKHEF, NL-3584 CB Utrecht, The Netherlands
 - 45 Purdue University, West Lafayette, IN 47907, USA
 - 46 Paul Scherrer Institut, PSI, CH-5232 Villigen, Switzerland
 - 47 DESY, D-15738 Zeuthen, FRG
 - 48 Eidgenössische Technische Hochschule, ETH Zürich, CH-8093 Zürich, Switzerland
 - 49 University of Hamburg, D-22761 Hamburg, FRG
 - 50 National Central University, Chung-Li, Taiwan, China
 - 51 Department of Physics, National Tsing Hua University, Taiwan, China
- [§] Supported by the German Bundesministerium für Bildung, Wissenschaft, Forschung und Technologie
[‡] Supported by the Hungarian OTKA fund under contract numbers T019181, F023259 and T024011.
[¶] Also supported by the Hungarian OTKA fund under contract numbers T22238 and T026178.
^b Supported also by the Comisión Interministerial de Ciencia y Tecnología.
[‡] Also supported by CONICET and Universidad Nacional de La Plata, CC 67, 1900 La Plata, Argentina.
[◇] Also supported by Panjab University, Chandigarh-160014, India.
[△] Supported by the National Natural Science Foundation of China.

References

- [1] S. L. Glashow, Nucl. Phys. **22** (1961) 579;
S. Weinberg, Phys. Rev. Lett. **19** (1967) 1264;
A. Salam, “Elementary Particle Theory”, Ed. N. Svartholm, Stockholm, Almquist and Wiksell, (1968), 367.
- [2] M. Veltman, Nucl. Phys. **B7** (1968) 637;
G. M. 't Hooft, Nucl. Phys. **B35** (1971) 167;
G. M. 't Hooft and M. Veltman, Nucl. Phys. **B44** (1972) 189; Nucl. Phys. **B50** (1972) 318.
- [3] M. Acciarri *et al.*, L3 Collaboration, Phys. Lett. **B403** (1997) 168.
- [4] M. Acciarri *et al.*, L3 Collaboration, Phys. Lett. **B436** (1998) 417.
- [5] R. Barate *et al.*, ALEPH Collaboration, Phys. Lett. **B462** (1999) 389.
- [6] P. Abreu *et al.*, DELPHI Collaboration, Phys. Lett. **B459** (1999) 382.
- [7] T. Tsukamoto and Y. Kurihara, Phys. Lett. **B389** (1996) 162.
- [8] B. Adeva *et al.*, L3 Collaboration, Nucl. Instr. Meth. **A289** (1990) 35; J. A. Bakken *et al.*, Nucl. Instr. Meth. **A275** (1989) 81; O. Adriani *et al.*, Nucl. Instr. Meth. **A302** (1991) 53; B. Adeva *et al.*, Nucl. Instr. Meth. **A323** (1992) 109; K. Deiters *et al.*, Nucl. Instr. Meth. **A323** (1992) 162; M. Chemarin *et al.*, Nucl. Instr. Meth. **A349** (1994) 345; M. Acciarri *et al.*, Nucl. Instr. Meth. **A351** (1994) 300; G. Basti *et al.*, Nucl. Instr. Meth. **A374** (1996) 293; A. Adam *et al.*, Nucl. Instr. Meth. **A383** (1996) 342.
- [9] J. Fujimoto *et al.*, Comp. Phys. Comm. **100** (1997) 128.
A standard parameter set including the G_μ renormalization scheme and the electromagnetic coupling $\alpha = 1/128.07$ is used. QED ISR corrections and an overall QCD correction factor $(1 + \alpha_s/\pi)$ for the hadronic W decay, using the value $\alpha_s = 0.120$, are applied.
- [10] F. A. Berends, R. Pittau and R. Kleiss, Comp. Phys. Comm. **85** (1995) 437.
A similar parameter set as for GRC4F is used.
- [11] M. Skrzypek *et al.*, Comp. Phys. Comm. **94** (1996) 216; M. Skrzypek *et al.*, Phys. Lett. **B372** (1996) 289.
- [12] S. Jadach, B. F. L. Ward and Z. Wąs, Comp. Phys. Comm. **79** (1994) 503.
- [13] J. H. Field, Phys. Lett. **B323** (1994) 432; J. H. Field and T. Riemann, Comp. Phys. Comm. **94** (1996) 53.
- [14] S. Jadach, W. Placzek and B. F. L. Ward, Phys. Lett. **B390** (1997) 298.
- [15] D. Karlen, Nucl. Phys. **B289** (1987) 23.
- [16] T. Sjöstrand, CERN-TH/7112/93 (1993), revised August 1995; T. Sjöstrand, Comp. Phys. Comm. **82** (1994) 74.
- [17] F. A. Berends and R. Kleiss, Nucl. Phys. **B253** (1985) 441.

- [18] R. Engel, Z.Phys. **C66** (1995) 203; R. Engel, J. Ranft and S. Roesler, Phys. Rev. **D52** (1995) 1459.
- [19] R. Brun *et al.*, preprint CERN DD/EE/84-1 (Revised 1987).
- [20] H. Fesefeldt, RWTH Aachen Report PITHA 85/02 (1985).
- [21] G. Passarino, hep-ph/0001212.
- [22] S. Catani *et al.*, Phys. Lett. **B269** (1991) 432;
S. Bethke *et al.*, Nucl. Phys. **B370** (1992) 310.
- [23] L. Lönnblad, C. Peterson and T. Rönkvallsson, Nucl. Phys. **B349** (1991) 675;
C. Peterson *et al.*, Comp. Phys. Comm. **81** (1994) 185.
- [24] W. Bartel *et al.*, JADE Collaboration, Z. Phys. **C33** (1986) 23;
S. Bethke *et al.*, Phys. Lett. **B213** (1988) 235.
- [25] R. Barate *et al.*, ALEPH Collaboration, Phys. Lett. **B422** (1998) 369;
M. Acciari *et al.*, L3 Collaboration, Phys. Lett. **B467** (1999) 171;
K. Ackerstaff *et al.*, OPAL Collaboration, Eur. Phys. J. **C8** (1999) 191.
- [26] B. Abbott *et al.*, DØ Collaboration, hep-ex/9912033, submitted to Phys. Rev. D;
F. Abe *et al.*, CDF Collaboration, Phys. Rev. Lett. **75** (1995) 1017.

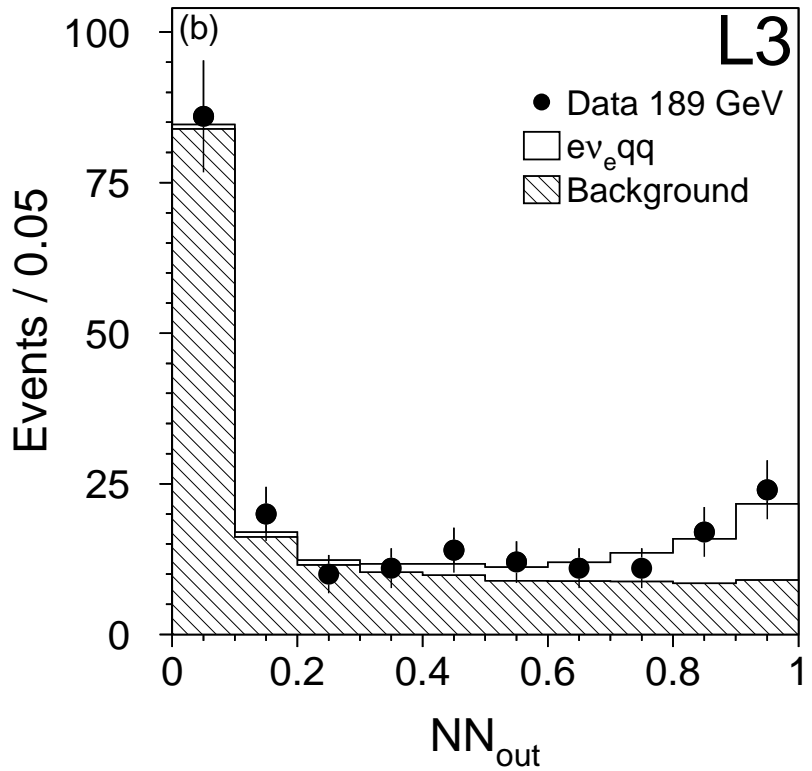
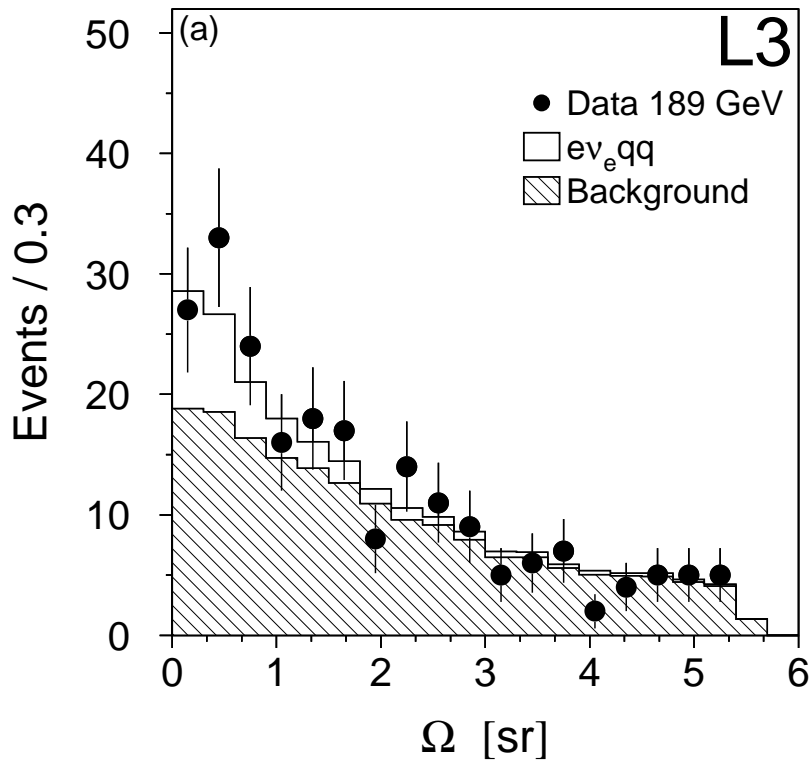


Figure 1: Distribution of (a) the 3-jet solid angle Ω and (b) the neural network output for the selected hadronic events. The points are data, the hatched histograms represent the background and the open histograms show the expected signal from $\nu_e qq$ final states as predicted by the EXCALIBUR Monte Carlo.

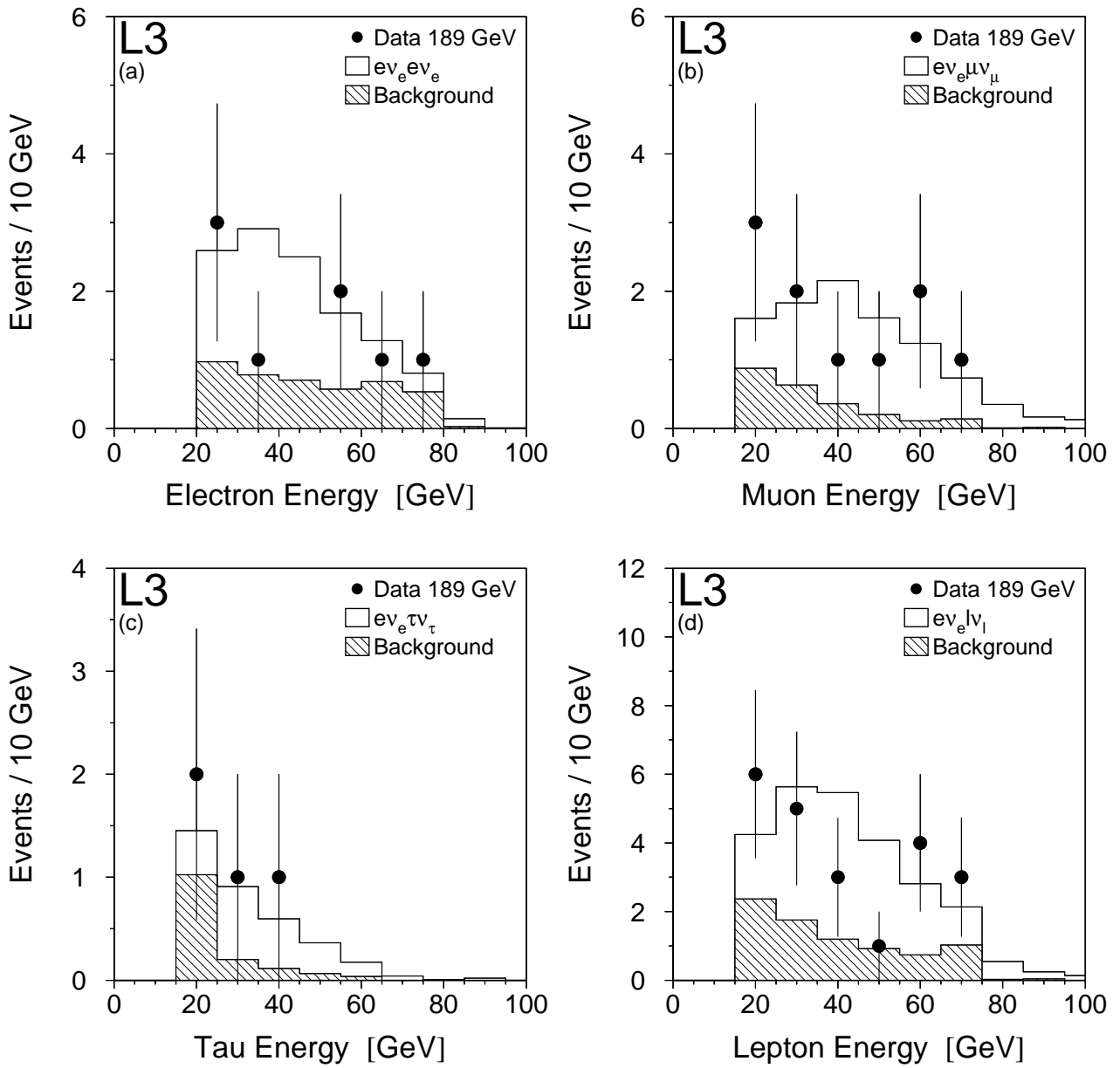


Figure 2: The energy spectra of the selected (a) single electron, (b) single muon, and (c) single tau candidates. The sum of the different lepton energy spectra is shown in (d). The points are data, the hatched histograms correspond to the background contribution. The open histograms show the expected signal from $\nu_e \ell \nu_\ell$ final states as predicted by the EXCALIBUR Monte Carlo.

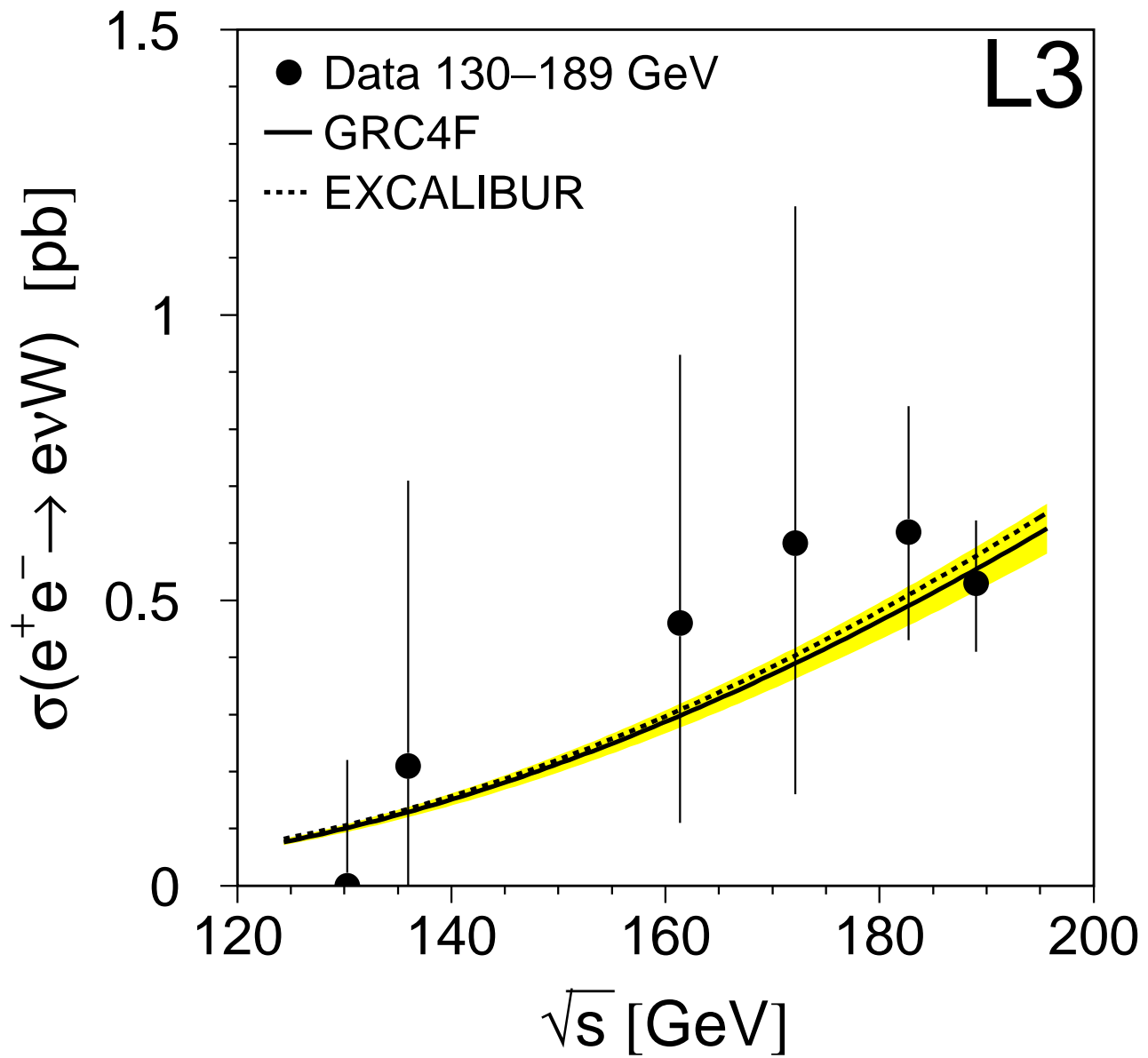


Figure 3: The measured cross-section of single W production within our phase-space cuts as a function of the centre-of-mass energy. The solid and dashed lines show predictions of the GRC4F and EXCALIBUR Monte Carlo programs, respectively. The estimated theoretical uncertainty of $\pm 7\%$ is indicated by the band.

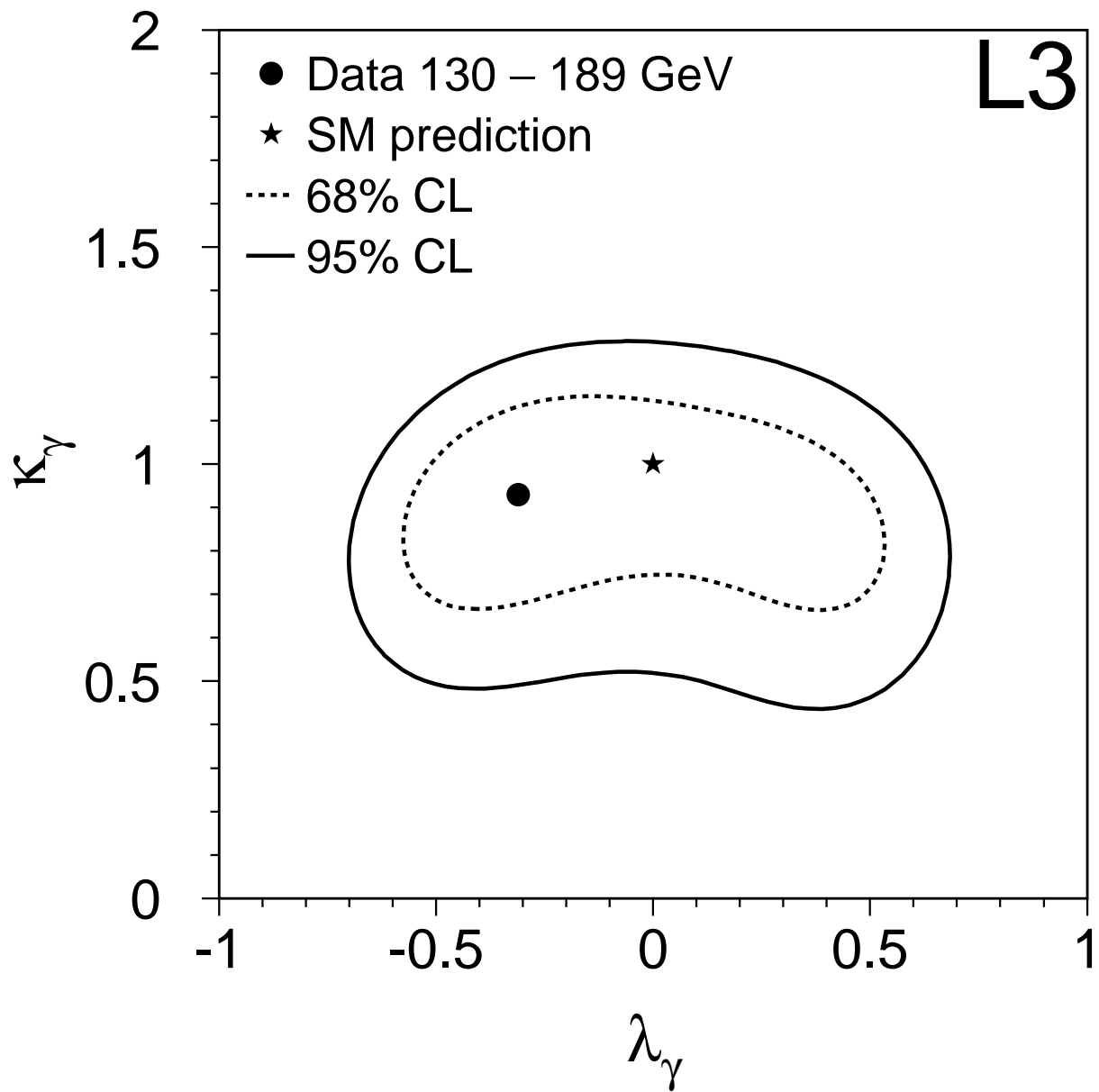


Figure 4: The contours corresponding to 68% and 95% confidence level in the $\kappa_\gamma - \lambda_\gamma$ plane. The point indicates the global minimum from the 2-parameter fit, to be compared with the Standard Model prediction indicated by the star.